Numerical solutions for a core–annular film fluid within a circular tube

Rodolfo Gallo and Said Kas–Danouche

Abstract. The nonlinear partial differential equation that models the evolution of the interface between two core–annular fluids within a circular cylinder of radius a and length L, is numerically solved using two finite difference schemes, one implicit and the other one explicit. Also, two pseudo–spectral schemes are used, one with Euler's method and the other one with Runge–Kutta's method of fourth order. The results of these methods are analized and compared considering the absolute error calculated with the infinite norm, the relative error, and the execution time. We find that the pseudo–spectral with Euler's method produces a very good numerical solution to the problem, considering the numerical solution obtained from the pseudo–spectral with Runge Kutta's method of fourth order as the most accurate numerical solution of the problem.

Resumen. La ecuación no lineal en derivadas parciales que modela la evolución de la interfaz entre dos fluidos núcleo–anulares dentro de un cilindro circular de radio a y de longitud L, es resuelto numéricamente utilizando dos esquemas en diferencias finitas, una implícita y la otra explícita. Además, se utilizan dos regímenes seudo–espectrales, uno con el método de Euler y el otro con un método de Runge–Kutta de cuarto orden. Los resultados de estos métodos se analizaron y se compararon considerando el error absoluto calculado con la norma infinito, el error relativo, y el tiempo de ejecución. Nos parece que el esquema pseudo–espectral con el método de Euler produce una muy buena solución numérica al problema, teniendo en cuenta la solución numérica obtenida de el esquema pseudo–espectral con el método de Runge Kutta de cuarto orden como la solución numérica más exacta del problema.

1 Introduction

The interface between two core–annular fluids within a circular cylinder was studied by Hammond [9]. He modeled the problem deducing the nonlinear partial differential equation $H_t = -\frac{1}{3}(H^3(H_{zzz} + H_z))_z$.

In 1934, Taylor [25] proved that the thread of unconfined fluids are decomposed into spheres. A year later, Tomotika [26] studied the case of a cylindrical thread of a viscous liquid suspended into another fluid, and Goren [7], in 1962, analyzed the linear stability of this problem. Hammond, in his work [9], extended Goren's study to a nonlinear regime. Also, he considered the dynamics of the problem, which it was not done before. Gauglitz & Radke [6] developed an alternative approximation based on Hammond's analysis including the exact expression of the curvature in the theory.

On the other hand, Chen, Bai, & Joseph [4] studied core–annular flows in vertical tubes considering the gravity, and including all the effects of viscosity stratification and interfacial tension. Renardy [21] studied core–annular flows of two fluids considering non axisymmetric instability. Kouris & Tsamopoulos [17] analized the dynamics of a flow of two phases of concentric immiscible fluids in a cylindrical tube. Later, Kas–Danouche [12] and Kas–Danouche, Papageorgiou, & Siegel [13], [15] studied the nonlinear interfacial stability of core–annular film flows with a constant pressure gradient and adding surfactants at the interface between the two fluids. In 2007, Kas–Danouche [14] considered the same problem studied by Hammond in [9], but he added insoluble surfactants at the interface between the two fluids, obtaining a new coupled system of two nonlinear partial differencial equations.

In this paper, a sketch of the derivation of the interface equation made by Hammond is presented. This equation is numerically solved using different numerical schemes: finite difference methods, explicit and implicit; also pseudo–spectral methods, one with Euler's method and another one with Runge–Kutta's method of fourth order, which is the relevant part of this work. A comparative analysis is made between the applied methods looking for the most convenient one. In the second section of this paper, the governing equations and the mathematical model developed by Hammond [9] are presented. This model consists in a nonlinear partial differential evolution equation. The numerical schemes are briefly introduced and the way how they are applied to the model is explained in the third section. In the fourth section, the numerical solutions are obtained when the methods previously proposed, are implemented. Several hundreds of numerical experiments were performed. They were mainly analyzed making use of the absolute and relative errors. Finally, we expose the conclusions. The results of this work will be used, in future researches, to validate numerical schemes that may be developed to solve the mathematical model obtained in [14].

2 Mathematical model and governing equations

We consider a film of an annular liquid surrounding a core fluid of length L, both concentric within a circular tube of radius a. The fluid in the film is of viscosity μ, while the core fluid has a viscosity $\lambda\mu$ and initial unperturbed radius b. The gravitational effects are neglected and we assume that no pressure gradients are applied to the system. So, the only force present is due to the interface tension γ which acts at the interface $\boldsymbol{S(r, z, \phi, t)}$ between the two fluids.

The mathematical model that we present, in this article, was developed by Hammond in [9]. We do not try in this article to redo all the derivation of the model, since the reader interested in it can find it in [9]. However, we mention some aspects oriented to the derivation of it.

2.1 Governing equations

Let us denote the velocity and the pressure in the annular fluid (film) as $\vec{\boldsymbol{u}}$ and $\boldsymbol{p}$, respectively. In the core fluid, the velocity and the pressure will be denoted by $\overrightarrow{\boldsymbol{U}}$ and $\boldsymbol{P}$. We will use cylindrical coordinates $\boldsymbol{(r, z, \phi)}$; the velocity components associated to these coordinates will be $\boldsymbol{(u, w, v)}$ in the film, and $\boldsymbol{(U, W, V)}$ in the core. At the interface $\boldsymbol{S(r, z, \phi, t)}$, the radial variable $\boldsymbol{r}$ will take the value

$$\boldsymbol{R(z, \phi, t) = a - h(z, \phi, t),} \tag{1}$$

where $\boldsymbol{h}$ is the thickness of the film.

The governing equations for this problem are the Navier–Stokes and continuity equations

$$\boldsymbol{\lambda\mu\nabla^2\overrightarrow{U} = \nabla P} \tag{2}$$

$$\boldsymbol{\nabla \cdot \overrightarrow{U} = 0,} \tag{3}$$

in the core fluid, where $\boldsymbol{R > r \geq 0}$, and

$$\boldsymbol{\mu\nabla^2\vec{u} = \nabla p} \tag{4}$$

$$\boldsymbol{\nabla \cdot \vec{u} = 0,} \tag{5}$$

in the film, where $\boldsymbol{a > r > R}$.

2.2 Boundary conditions

The imposed boundary conditions satisfy the physical problem to be modeled. They are: No slip condition at the pipe wall

$$\boldsymbol{\vec{u} = 0} \text{ in } \boldsymbol{r = a,}$$

continuity of velocity at the interface

$$\vec{u} = \overrightarrow{U} \text{ in } r = R,$$

normal stress balance

$$\vec{n} \cdot \sigma \cdot \vec{n} - \vec{n} \cdot \Sigma \cdot \vec{n} = \vec{n}\gamma\kappa\vec{n},$$

tangential stress balance

$$\vec{t} \cdot \sigma \cdot \vec{n} - \vec{t} \cdot \Sigma \cdot \vec{n} = \vec{t}\gamma\kappa\vec{n},$$

where γ is the interfacial tension coefficient, $\vec{n}$ is the normal vector to the interface and pointing out the annular fluid, $\vec{t}$ is the tangential vector at the interface, σ and Σ are the stress tensors given by

$$\begin{aligned} \sigma &= -pI + \mu(\nabla\vec{u} + \nabla\vec{u}^T), \\ \Sigma &= -PI + \lambda\mu(\nabla\overrightarrow{U} + \nabla\overrightarrow{U}^T), \end{aligned}$$

with I as the identity matrix of order 3, $.^T$ denotes the transposed, and

$$\kappa = \nabla \cdot \hat{n}, \tag{6}$$

is the mean curvature of the interface, where $\hat{n} = \frac{\vec{n}}{|\vec{n}|}$.

Also, the kinematic condition is required

$$u = -h_t - \vec{u} \cdot \nabla h = -h_t - wh_z - v\frac{h_\phi}{r},$$

which, rearranging terms, it takes the form,

$$h_t = -u - wh_z - v\frac{h_\phi}{a-h} \quad \text{at} \quad S(r, z, \phi, t). \tag{7}$$

This way, the evolution equation for the interface will be completely determined by (7), if the components of the velocity are known.

In what follows, all independent and dependent variables are non–dimensionalized, and asymptotic approximations are used to obtain the evolution equation of the interface. The thickness of the unperturbed film is $a - b$. We introduce the small non–dimensional parameter ϵ

$$\epsilon = \frac{a-b}{a}.$$

Now, it is assumed that $\epsilon << 1$ and $\epsilon\lambda << 1$, $h(z,t)/\epsilon a = O(1)$ and $a\partial/\partial z = O(1)$. Taking into account certain estimations which Hammond, in

[9], introduces; we define the following variables, denoting the non–dimensional variables with asterisks. In the film we take the independent variables

$$z^* = \frac{z}{a}; \quad y^* = \frac{a-r}{\epsilon a}; \quad t^* = \frac{t}{\epsilon^{-3}(a\mu/\gamma)}.$$

So, from (1) the interface can be described by

$$y^* = \frac{h(z,t)}{\epsilon a} = H^*(z^*, t^*),$$

with $H^* = O(1)$. Also, the radial and axial velocities, and the pressure are expressed in non–dimensional form.

Considering the non–dimensional form of (4)–(5) and eliminating the asterisks from the notation, we obtain

$$\begin{aligned} w_z - u_y &= -\epsilon u + O(\epsilon^2), \\ p_y &= -\epsilon^2 u_{yy} + O(\epsilon^3), \\ p_z - w_{yy} &= -\epsilon w_y + O(\epsilon^2). \end{aligned}$$

Similarly, the boundary conditions are non–dimensionalized. In this way, the non–dimensional tangential stress balance takes the following form

$$\begin{aligned} & \epsilon^2\Big((1-\epsilon^2 H_z^2)(-w_y + \epsilon^2 u_z) + 2\epsilon^2 H_z(u_y - w_z)\Big) \\ = \;& \lambda\epsilon^3\Big((1-\epsilon^2 H_z^2)(U_z+W_r) + 2\epsilon H_z(W_z - U_r)\Big), \text{ in } S(r,z,t); \end{aligned}$$

from which we obtain

$$w_y(H,z) = -\epsilon\lambda(U_z + W_r) + O(\epsilon^2, \epsilon^2\lambda).$$

Now, we non–dimensionalize the normal stress balance, obtaining

$$\begin{aligned} & |\,\vec{n}\,|^2 - \epsilon\,|\,\vec{n}\,|^2\, p + 2\Big(-\epsilon^3 u_y + \epsilon^5 H_z u_z - \epsilon^3 H_z w_y + \epsilon^5 H_z^2 w_z\Big) \\ - \;& \lambda\epsilon^3\Big(-|\,\vec{n}\,|^2\, P + 2U_r + 2\epsilon H_z U_z + 2\epsilon H_z W_r + 2\epsilon^2 H_z^2 W_z\Big) \\ = \;& |\vec{n}|^2\Big((1+\epsilon^2 H_z^2)^{-\frac{1}{2}}(1-\epsilon H)^{-1} + \epsilon H_{zz}(1+\epsilon^2 H_z^2)^{-\frac{3}{2}}\Big), \text{ in } S \end{aligned}$$

from which results

$$P(H(z,t),z) = -(H + H_{zz}) + O(\epsilon^2, \epsilon^2\lambda).$$

Next, we non–dimensionalize the equation (7), which is the kinematic condition, to obtain:

$$H_t = -u - wH_z. \tag{8}$$

At this point, Hammond [9] introduces asymptotic expansions into the whole problem and consider only the high order terms (O(1)). From that we obtain $\boldsymbol{w}$ and $\boldsymbol{u}$, which when are substituted in (8) give as a result the nonlinear partial differential evolution equation for the interface

$$\boldsymbol{H_t = -\frac{1}{3}(H^3(H_z + H_{zzz}))_z,} \tag{9}$$

which, in this paper, we call it the Hammond's equation. In [14], Kas–Danouche obtained a system of two coupled non linear partial differential equations, one for the interface evolution and the other one for the evolution of the surfactant concentration. When the surfactant concentration is set equal to zero, we obtain the equation (9). So, the results of this paper will help us to validate the numerical results of the system derived in [14], which it will be the core for future researches.

2.3 The rescaled Hammond's equation

With the goal of simplifying the numerical calculations, we rescale $\boldsymbol{z}$ from $\boldsymbol{[0, L]}$ to the interval $\boldsymbol{[0, 2\pi]}$. In order to do this, we consider the change of variables $\boldsymbol{z = \frac{2\pi}{L}\tilde{z}}$ and $\boldsymbol{t = (\frac{2\pi}{L})^2\tilde{t}}$, where $\boldsymbol{\tilde{z} \in [0, L]}$, $\boldsymbol{\tilde{t} \geq 0}$ and the variables with "˜" represent the unscaled variables. Thus, we have $\boldsymbol{z \in [0, 2\pi]}$, $\boldsymbol{t \geq 0}$, and (9) expressed in the new variables as

$$\boldsymbol{H_t = -\frac{1}{3}(H^3(\lambda^2 H_{zzz} + H_z))_z,} \tag{10}$$

where $\boldsymbol{\lambda = \frac{2\pi}{L}}$.

The initial condition for the rescaled problem is

$$\boldsymbol{H(z, 0) = 1 + \beta \cos z, \quad 0 \leq z \leq 2\pi,} \tag{11}$$

where $\boldsymbol{\beta > 0}$.

The numerical schemes to be developed in the next section will be applied to the equation (10) with the initial condition (11), in the interval $\boldsymbol{0 \leq z \leq 2\pi}$, at time $\boldsymbol{t}$.

3 Numerical schemes

In this section, four schemes are developed to be applied to the interface equation (10). Two of them use finite differences for both spatial and temporal variables, one explicit and the other one implicit. The other two schemes are based on pseudo–spectral methods [2], making use of the Euler's method, in one of them, and the Runge Kutta's method of fourth order in the other one.

In order to numerically solve the partial differential equation for the evolution of the interface, certain initial and boundary conditions are imposed. The boundary conditions that Hammond [9] considered are:

$$\frac{\partial^{2j+1}\boldsymbol{H}}{\partial \boldsymbol{z}^{2j+1}} = \boldsymbol{0}, \quad \text{with} \qquad \boldsymbol{j} = \boldsymbol{0}, \boldsymbol{1}, \boldsymbol{2}, \ldots; \boldsymbol{z} = \boldsymbol{0}, \frac{\boldsymbol{1}}{\boldsymbol{2}}\boldsymbol{L}, \tag{12}$$

which correspond to $\boldsymbol{H}$ even, with period $\boldsymbol{L}$ and reflectionally symmetric about $\boldsymbol{z} = \frac{\boldsymbol{1}}{\boldsymbol{2}}\boldsymbol{L}$.

3.1 Finite differences

Here, we suppose that $\boldsymbol{H}$ is sufficiently smooth that admit Taylor's expansions for $\boldsymbol{H}(\boldsymbol{z}+\boldsymbol{h}, \boldsymbol{t})$ and $\boldsymbol{H}(\boldsymbol{z}-\boldsymbol{h}, \boldsymbol{t})$ at point $(\boldsymbol{z}, \boldsymbol{t})$ [1]. Therefore, we can write the finite difference approximations for $\boldsymbol{H_z}$, $\boldsymbol{H_{zz}}$, $\boldsymbol{H_{zzz}}$, and $\boldsymbol{H_{zzzz}}$ as follows

$$\boldsymbol{H_z} \approx \frac{\boldsymbol{H}(\boldsymbol{z}+\boldsymbol{h}, \boldsymbol{t}) - \boldsymbol{H}(\boldsymbol{z}-\boldsymbol{h}, \boldsymbol{t})}{\boldsymbol{2h}}, \tag{13}$$

$$\boldsymbol{H_{zz}} \approx \frac{\boldsymbol{H}(\boldsymbol{z}-\boldsymbol{h}, \boldsymbol{t}) - \boldsymbol{2H}(\boldsymbol{z}, \boldsymbol{t}) + \boldsymbol{H}(\boldsymbol{z}+\boldsymbol{h}, \boldsymbol{t})}{\boldsymbol{h^2}}. \tag{14}$$

From the equations (13) and (14), we obtain

$$\begin{aligned} \boldsymbol{H_{zzz}} = (\boldsymbol{H_z})_{\boldsymbol{zz}} &\approx \frac{\boldsymbol{1}}{\boldsymbol{2h^3}}\Big(\boldsymbol{H}(\boldsymbol{z}+\boldsymbol{2h}, \boldsymbol{t}) - \boldsymbol{2H}(\boldsymbol{z}+\boldsymbol{h}, \boldsymbol{t}) \\ &+ \boldsymbol{2H}(\boldsymbol{z}-\boldsymbol{h}, \boldsymbol{t}) - \boldsymbol{H}(\boldsymbol{z}-\boldsymbol{2h}, \boldsymbol{t})\Big). \end{aligned} \tag{15}$$

From the equation (14) we have

$$\begin{aligned} \boldsymbol{H_{zzzz}} = (\boldsymbol{H_{zz}})_{\boldsymbol{zz}} &\approx \frac{\boldsymbol{1}}{\boldsymbol{h^4}}\Big((\boldsymbol{H}(\boldsymbol{z}-\boldsymbol{2h}, \boldsymbol{t}) - \boldsymbol{4H}(\boldsymbol{z}-\boldsymbol{h}, \boldsymbol{t}) + \boldsymbol{6H}(\boldsymbol{z}, \boldsymbol{t}) \\ &- \boldsymbol{4H}(\boldsymbol{z}+\boldsymbol{h}, \boldsymbol{t}) + \boldsymbol{H}(\boldsymbol{z}+\boldsymbol{2h}, \boldsymbol{t})\Big). \end{aligned} \tag{16}$$

On the other hand, for all $\boldsymbol{k} \neq \boldsymbol{0}$, at the point $(\boldsymbol{z}, \boldsymbol{t})$ we use finite differences for the time derivative to obtain the expression

$$\boldsymbol{H}(\boldsymbol{z}, \boldsymbol{t}+\boldsymbol{k}) \approx \boldsymbol{H}(\boldsymbol{z}, \boldsymbol{t}) + \boldsymbol{k}\boldsymbol{H_t}, \tag{17}$$

to approximate $\boldsymbol{H_t}$, where $\boldsymbol{k}$ is the time step.

3.1.1 Explicit scheme In what follows we develop the explicit scheme [23] to be applied to the interface evolution equation (10). We uniformly particionate the intervals $\mathbf{0} \leq \boldsymbol{z} \leq \mathbf{2\pi}$ and $\mathbf{0} \leq \boldsymbol{t} \leq \boldsymbol{T}$, in $\boldsymbol{n}$ and $\boldsymbol{m}$ sub–intervals, respectively. The stepsize in $\boldsymbol{z}$ will be denoted by $\boldsymbol{\Delta z}$, and the stepsize in $\boldsymbol{t}$ by $\boldsymbol{\Delta t}$.

The rescaled interface evolution equation (10) can be rewritten in an expanded form as

$$\boldsymbol{H_t = -\frac{1}{3}\Big(3H^2H_z(\lambda^2H_{zzz} + H_z) + H^3(\lambda^2H_{zzzz} + H_{zz})\Big).} \tag{18}$$

Substituting the finite difference approximations (13)-(17) for the partial derivatives in (18), we obtain

$$\begin{aligned}
\boldsymbol{H}\ \ \boldsymbol{(z, t+\Delta t)} \approx\ & \boldsymbol{-\frac{\Delta t\lambda^2}{3(\Delta z)^4}H^2(z,t)\Bigg[\frac{3}{4}\Big(H(z+\Delta z,t) - H(z-\Delta z,t)\Big).}\\
& \boldsymbol{\Big[H(z+2\Delta z,t) - H(z-2\Delta z,t) + \left(\frac{(\Delta z)^2}{\lambda^2} - 2\right)\Big(H(z+\Delta z,t) - H(z-\Delta z,t)\Big)\Big]}\\
& \boldsymbol{+\ \ H(z,t)\Big[H(z-2\Delta z,t) + H(z+2\Delta z,t) + \left(\frac{(\Delta z)^2}{\lambda^2} - 4\right)\Big(H(z-\Delta z,t)}\\
& \boldsymbol{+\ \ H(z+\Delta z,t)\Big) + \left(6 - 2\frac{(\Delta z)^2}{\lambda^2}\right)H(z,t)\Big]\Bigg] + H(z,t).}
\end{aligned}$$

Re–writing the equation using the notation

$$\boldsymbol{H_{i+\tilde{n},j+\tilde{m}} = H(z_i + \tilde{n}\Delta z, t_j + \tilde{m}\Delta t)}$$

, for $\boldsymbol{\tilde{n}, \tilde{m} = 0, 1, 2}$, we have

$$\begin{aligned}
\boldsymbol{H_{i,j+1}} \ \ =\ \ & \boldsymbol{L_1H_{i,j}^2\Big(\frac{3}{4}(H_{i+1,j} - H_{i-1,j})\Big(H_{i+2,j} - H_{i-2,j} + L_2(H_{i+1,j} - H_{i-1,j})\Big)}\\
& \boldsymbol{+H_{i,j}\Big(H_{i-2,j} + H_{i+2,j} + L_3(H_{i-1,j} + H_{i+1,j}) + L_4H_{i,j}\Big)\Big) + H_{i,j},}
\end{aligned} \tag{19}$$

where $\boldsymbol{L_1 = -\frac{1}{3}\frac{\Delta t\lambda^2}{(\Delta z)^4}}$, $\boldsymbol{L_2 = \frac{(\Delta z)^2}{\lambda^2} - 2}$, $\boldsymbol{L_3 = \frac{(\Delta z)^2}{\lambda^2} - 4}$ and $\boldsymbol{L_4 = 6 - 2\frac{(\Delta z)^2}{\lambda^2}}$.

The equation (19) is the explicit representation in finite differences for the interface evolution equation. In order to find the value of $\boldsymbol{H}$ at the point $\boldsymbol{(z_i, t_{j+1})}$, this scheme requires the values of $\boldsymbol{H}$ at five spatial points $\boldsymbol{z_i}$ at time $\boldsymbol{t_j}$, as is shown in the following diagram of points

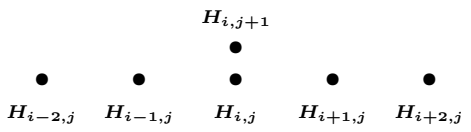

The initial condition (11) gives the values of $\boldsymbol{H_{i,0}}$; i.e.,

$$\boldsymbol{H_{i,0} = 1 + \beta\cos(z_i),\ \ i = 0,\ldots,n-1.}$$

From the equation (19) we obtain the values of $\boldsymbol{H}$ at the nodes $\boldsymbol{z_i}$, $\boldsymbol{i = 0,...,n-1}$ and times $\boldsymbol{t_{j+1}}$, $\boldsymbol{j = 0,1...}$. The boundary conditions suggest that $\boldsymbol{H}$ has to be periodic of period $\boldsymbol{2\pi}$ (after rescaling $\boldsymbol{z}$ from $\boldsymbol{[0,L]}$ to $\boldsymbol{[0,2\pi]}$), and symmetric with respect to $\boldsymbol{z = 0}$. Therefore, at the nodes of the boundary we have

$$\begin{aligned} &\boldsymbol{H_{-2,j} = H_{2,j},\ H_{-1,j} = H_{1,j}}, && \boldsymbol{j = 0,\ldots,m} \\ &\boldsymbol{H_{n,j} = H_{0,j},\ H_{n+1,j} = H_{1,j}}, && \boldsymbol{H_{n+2,j} = H_{2,j},\quad j = 0,\ldots,m.} \end{aligned}$$

3.1.2 Implicit scheme The implicit scheme that we develop here acts on the nonlinear term of higher order of the interface evolution equation; i.e, $\boldsymbol{H_{zzzz}}$ is considered to be found for times $\boldsymbol{t_{j+\frac{1}{2}}}$ and $\boldsymbol{t_{j+1}}$. For this, is convenient to write the equation (10) in terms of the higher order derivative, as follows

$$\boldsymbol{H_t = -\frac{1}{3}\lambda^2 H^3 H_{zzzz} - f(H, H_z, H_{zz}, H_{zzz}),}$$

where

$$\boldsymbol{f(H, H_z, H_{zz}, H_{zzz}) = \frac{1}{3}H^3 H_{zz} + \lambda^2 H^2 H_z H_{zzz} + H^2 H_z^2.}$$

The equation (10) will be solved numerically in the interval $\boldsymbol{0 \le z \le 2\pi}$, under the initial condition

$$\boldsymbol{H(z,0) = 1 + \beta\cos(z),} \qquad \boldsymbol{z \in [0,2\pi],} \tag{20}$$

and the boundary conditions

$$\begin{aligned} \boldsymbol{H_{-1,j} = H_{n-1,j},} \qquad & \boldsymbol{H_{0,j} = H_{n,j},\quad H_{1,j} = H_{n+1,j},} \\ \boldsymbol{H_{2,j} = H_{n+2,j},} \qquad & \boldsymbol{H_{3,j} = H_{n+3,j},} \end{aligned} \tag{21}$$

which guarantee the periodicity of the solution.

The implicit scheme in finite differences that we propose is based on the implicit scheme proposed by Kas–Danouche in [14]:

$$\boldsymbol{\frac{H^{j+\frac{1}{2}} - H^j}{\frac{\Delta t}{2}} = -\frac{1}{3}\lambda^2 (H^j)^3 H^{j+\frac{1}{2}}_{zzzz} - f^j(H^j, H^j_z, H^j_{zz}, H^j_{zzz})} \tag{22}$$

$$\begin{aligned} \boldsymbol{\frac{H^{j+1} - H^j}{\Delta t}} &= \boldsymbol{-\frac{1}{3}\lambda^2 (H^{j+\frac{1}{2}})^3 \Big(\frac{H^{j+1}_{zzzz} + H^j_{zzzz}}{2\Delta z}\Big)} \\ &- \boldsymbol{f^{j+\frac{1}{2}}(H^{j+\frac{1}{2}}, H^{j+\frac{1}{2}}_z, H^{j+\frac{1}{2}}_{zz}, H^{j+\frac{1}{2}}_{zzz}).} \end{aligned} \tag{23}$$

It is a scheme of half step that uses forward finite differences for the time integration, where (22) is the predictor and (23) is the corrector. Using (22) we find $\boldsymbol{H}$ computed for time $\boldsymbol{t_{j+\frac{1}{2}}}$. Using (23) we improve $\boldsymbol{H}$ computed in the next half step after the predictor is used. It corresponds to $\boldsymbol{H}$ for time $\boldsymbol{t_{j+1}}$, using Crank–Nicolson [18] for $\boldsymbol{H_{zzzz}}$ and centered finite differences for all the spatial derivatives.

In the equations (22) and (23), the notation $\boldsymbol{H^{j+\frac{1}{2}}}$, $\boldsymbol{j = 0, 1}$, means $\boldsymbol{H}$ evaluated at $\boldsymbol{(z, t_{j+\frac{1}{2}})}$. Now, we use the notation $\boldsymbol{H_{i,j+\frac{1}{2}}}$, to make reference to $\boldsymbol{H}$ evaluated at $\boldsymbol{(z_i, t_{j+\frac{1}{2}})}$, $\boldsymbol{j = 0, 1}$. Substituting (16) into (22), we obtain

$$\begin{aligned}\frac{\boldsymbol{H_{i,j+\frac{1}{2}} - H_{i,j}}}{\frac{\boldsymbol{\Delta t}}{\boldsymbol{2}}} &= -\frac{\boldsymbol{\lambda^2 H_{i,j}^3}}{\boldsymbol{3(\Delta z)^4}}\Big(\boldsymbol{H_{i-2,j+\frac{1}{2}} - 4H_{i-1,j+\frac{1}{2}} + 6H_{i,j+\frac{1}{2}}} \\ &\quad \boldsymbol{-4H_{i+1,j+\frac{1}{2}} + H_{i+2,j+\frac{1}{2}}}\Big) \\ &\quad \boldsymbol{-f_i^j(H^j, H_z^j, H_{zz}^j, H_{zzz}^j),} \end{aligned} \tag{24}$$

where,

$$\begin{aligned}\boldsymbol{f_i^j} &= \boldsymbol{\frac{1}{3}H_{i,j}^3 H_{zz}(z_i, t_j)\lambda^2 H_{i,j}^2 H_z(z_i, t_j) H_{zzz}(z_i, t_j)} \\ &\quad \boldsymbol{+H_{i,j}^2 H_z^2(z_i, t_j).}\end{aligned}$$

For each fixed $\boldsymbol{j}$, we denote

$$\boldsymbol{C_i = -\frac{(\Delta t)\lambda^2 H_{i,j}^3}{6(\Delta z)^4}, \;\; i = 0, 1, \ldots, n-1,}$$

so that (24) takes the form

$$\begin{aligned}\boldsymbol{-C_i H_{i-2,j+\frac{1}{2}}} &+ \boldsymbol{4C_i H_{i-1,j+\frac{1}{2}} + (1 - 6C_i) H_{i,j+\frac{1}{2}} + 4C_i H_{i+1,j+\frac{1}{2}}} \\ \boldsymbol{-C_i H_{i+2,j+\frac{1}{2}}} &= \boldsymbol{H_{i,j} - \frac{\Delta t}{2} f_i^j(H^j, H_z^j, H_{zz}^j, H_{zzz}^j),}\end{aligned} \tag{25}$$

for values of $\boldsymbol{i = 0, \ldots, n-1}$. This equation along with the initial and boundary conditions given by (20) and (21), respectively, can be expressed in the matricial form

$$\boldsymbol{A^j H^{j+\frac{1}{2}} = b^j, \quad j = 1, \ldots, M,} \tag{26}$$

where $\boldsymbol{A^j}$ is the coefficient matrix of the system of equations (25). $\boldsymbol{A^j}$ is of order $\boldsymbol{n}$, $\boldsymbol{H^{j+\frac{1}{2}}}$ is the column vector of order $\boldsymbol{n}$, corresponding to the solution we want to calculate for time $\boldsymbol{t_{j+\frac{1}{2}}}$, and $\boldsymbol{b^j}$ is the vector corresponding to the right hand side of the system of equations.

In a similar way, substituting (16) in (23), we have

$$\begin{aligned} -c_i' H_{i-2,j+1} &+4c_i' H_{i-1,j+1} + (1-6c_i') H_{i,j+1} \\ &+4c_i' H_{i+1,j+1} - c_i' H_{i+2,j+1} \\ = \;& c_i'(H_{i-2,j} - 4H_{i-1,j} + 6H_{i,j} - 4H_{i+1,j} + H_{i+2,j}) \\ &-(\Delta t) f_i^{j+\frac{1}{2}} + H_{i,j}, \end{aligned}$$

where

$$c_i' = -\frac{(\Delta t)\lambda^2 H_{i,j+\frac{1}{2}}^3}{6(\Delta z)^4}, i = 0, \ldots, n-1.$$

This equation, along with the initial and boundary conditions (20) and (21), respectively, produces the matricial system

$$B^{j+\frac{1}{2}} H^{j+1} = a, \quad j = 1, \ldots, M. \tag{27}$$

For each fixed j, $B^{j+\frac{1}{2}}$ is the matrix of order n, which can be obtained substituting C_i by c_i' in the matrix A^j of the system (26). H^{j+1} is the column vector of order n, corresponding to the solution we want to calculate for time t_{j+1}, and a is the vector corresponding to the right hand side of the system of equations.

For each $j = 1, ..., M$, the systems of equations (26) and (27) are solved using the method of Woodbury [20], which transforms the almost pentadiagonal matrices to pentadiagonal matrices.

3.2 Pseudo–spectral methods

These methods use the Fourier Transforms for the calculation of the spatial derivatives. For the time derivative a different method, usually finite differences, is used. This is why they are classified as pseudo–spectral methods [2]. The application of these methods is justified, in the first place, because the solution of the interface equation is a smooth function, periodic in the spatial variable and it can be approximated using a finite sum as $H(z,t) = \sum_{n=-N}^{N} h_n(t) e^{inz}$. In the second place, by the periodicity caracter of the initial condition. Computations of the spatial derivatives involved in the nonlinear terms are made in the spectral space. The connection between the spectral space and the physical space is made using the Fast Fourier Transform (FFT) and the Inverse Fast Fourier Transform (IFFT). The errors of the spectral methods are exponentially smalls [2], [8], and this is the main reason why we apply them to our problem.

In this section, two pseudo–spectral schemes are proposed for the integration with respect to time. One scheme uses the Euler's method and the other one uses the Runge Kutta's method of fourth order [1], [5].

In the rescaled Hammond equation (10), let us call

$$\begin{aligned} \boldsymbol{R(z,t)} &= -\frac{\mathbf{1}}{\mathbf{3}}\Big(\boldsymbol{H^3(\lambda^2 H_{zzz} + H_z)}\Big)_{\boldsymbol{z}} \\ &= -\boldsymbol{H^2 H_z(\lambda^2 H_{zzz} + H_z)} - \frac{\mathbf{1}}{\mathbf{3}}\boldsymbol{H^3(\lambda^2 H_{zzzz} + H_{zz}).} \quad (28) \end{aligned}$$

Suppose that both $\boldsymbol{H(z,t)}$ and $\boldsymbol{R(z,t)}$ admit each one a developing Fourier series [11]

$$\begin{aligned} \boldsymbol{H(z,t)} &= \sum_{n=-\infty}^{\infty} \boldsymbol{h_n(t)e^{inz}} \quad (29) \\ \boldsymbol{R(z,t)} &= \sum_{n=-\infty}^{\infty} \boldsymbol{r_n(t)e^{inz}.} \end{aligned}$$

In the equation (29), the partial derivative $\frac{\partial \boldsymbol{H}}{\partial \boldsymbol{t}}$, is obtained deriving the series term by term; then the equation (10) can be written in the form

$$\sum_{n=-\infty}^{\infty} \frac{\partial \boldsymbol{h_n}}{\partial \boldsymbol{t}}\boldsymbol{(t)e^{inz}} = \sum_{n=-\infty}^{\infty} \boldsymbol{r_n(t)e^{inz}.}$$

These series coincide if the coefficients of $\boldsymbol{e^{inz}}$ are both equal term by term. Therefore, we obtain the system of ordinary differential equations

$$\frac{\boldsymbol{dh_n}}{\boldsymbol{dt}}\boldsymbol{(t) = r_n(t).} \quad (30)$$

The system (30) is numerically solved for values of $\boldsymbol{n = \frac{-N}{2} + 1, ..., \frac{N}{2}}$, with $\boldsymbol{N}$ a natural number, using the Euler's method and the Runge Kutta's method of fourth order [1], [5].

3.2.1 Pseudo–spectral with Euler's method For the Euler's method we write

$$\boldsymbol{h_n(t_{i+1}) = h_n(t_i) + (\Delta t) r_n(t_i),} \quad \text{for } \boldsymbol{i = 0, 1, ...} \quad (31)$$

The coefficients $\boldsymbol{h_n(t)}$ of $\boldsymbol{H(z,t)}$, in (29), are calculated applying the Fast Fourier Transform (FFT) to a set of values of $\boldsymbol{H(z,t)}$ in the interval $\boldsymbol{[0, 2\pi]}$ at equidistant points $\boldsymbol{z_j = j(\Delta z)}$, $\boldsymbol{\Delta z = \frac{2\pi}{N}}$, $\boldsymbol{j = 0, ..., N-1}$. The value of the partial derivatives $\boldsymbol{H_z, H_{zz}, H_{zzz}, H_{zzzz}}$, at the points $\boldsymbol{z_j}$, are obtained calculating $\boldsymbol{\frac{\partial}{\partial z}, \ldots, \frac{\partial^4}{\partial z^4}}$ at the right hand side of (29) term by term, and applying later the Inverse Fast Fourier Transform (IFFT).

In order to obtain the initial condition, we apply FFT to the initial condition, which is given by $\boldsymbol{H_0 = H(z,0) = 1 + \frac{1}{2}\cos z}$, to obtain the $\boldsymbol{h_n(0)}$.

3.2.2 Pseudo–spectral with Runge Kutta's method of fourth order Here we solve the system of equations (30) using the Runge–Kutta's method of fourth order (RK).

For an initial value problem as

$$\boldsymbol{y' = f(t, y), \quad y(t_0) = y_0,}$$

the RK method is given by

$$\boldsymbol{y_{k+1} = y_k + \frac{1}{6}(f_1 + 2f_2 + +2f_3 + f_4),}$$

where

$$\begin{aligned} \boldsymbol{f_1} &= \boldsymbol{(\Delta t) f(t_k, y_k),} \\ \boldsymbol{f_2} &= \boldsymbol{(\Delta t) f(t_k + \frac{\Delta t}{2}, y_k + \frac{1}{2} f_1),} \\ \boldsymbol{f_3} &= \boldsymbol{(\Delta t) f(t_k + \frac{\Delta t}{2}, y_k + \frac{1}{2} f_2),} \\ \boldsymbol{f_4} &= \boldsymbol{(\Delta t) f(t_k + \Delta t, y_k + f_3).} \end{aligned}$$

Thus, the following value $\boldsymbol{y_{k+1}}$ is determined by the current value $\boldsymbol{y_k}$ plus a weighted average of slopes. The RK method is a fourth order method which means that the error at each step is of order $\boldsymbol{(\Delta t)^5}$, while the accumulated total error has order $\boldsymbol{(\Delta t)^4}$.

In our case, as $\boldsymbol{r_n}$ is a function obtained applying FFT to

$$\boldsymbol{R(H, H_z, H_{zz}, H_{zzz}, H_{zzzz})}$$

in (28), and $\boldsymbol{H}$ is obtained applying IFFT to $\boldsymbol{h}$ in (29), the equation (30) can be written, eliminating $\boldsymbol{n}$, as

$$\boldsymbol{h' = f(h),} \tag{32}$$

where

$$\boldsymbol{f(h) = FFT(R(IFFT(h))).}$$

Therefore, we apply RK to the equation (32), with the initial condition

$$\boldsymbol{h_0 = FFT(H_0).}$$

4 Numerical solutions

All the methods used in this article were coded using MatLab. The code for the explicit finite difference method is identified as EXPLI. We have called the code

for the implicit finite difference method as IMPLI. We use the name SPEC_EU to identify the code for the pseudo–spectral with Euler's method and SPEC_RK to represent the code for the pseudo–spectral with Runge Kutta's method of fourth order. The codes depend on certain parameters: a) the length $\boldsymbol{L}$ of the tube, the variable $\boldsymbol{z}$ is rescaled from the interval $[\mathbf{0}, \boldsymbol{L}]$ to the interval $[\mathbf{0}, \mathbf{2\pi}]$, the graphs of the calculated solutions are shown in the interval $[\mathbf{0}, \mathbf{2\pi}]$, but the solution in the interval $[\mathbf{0}, \boldsymbol{L}]$ can be recovered multiplying z by $\frac{\boldsymbol{L}}{\mathbf{2\pi}}$; b) the final time $\boldsymbol{T}$, the solutions were calculated for $\boldsymbol{T} = \mathbf{0, 6, 18, 30, 60}$, observing that for values of $\boldsymbol{T} > \mathbf{60}$, the solutions do not change too much from that for $\boldsymbol{T} = \mathbf{60}$, c) $\boldsymbol{N}$ is another parameter, which represents the number of sub–intervals, with the same length, in which the interval $[\mathbf{0}, \mathbf{2\pi}]$ is sub–divided. For the case of the pseudo–spectral methods, $\boldsymbol{N}$ must be chosen as a power of 2; d) $\boldsymbol{\lambda} = \frac{\mathbf{2\pi}}{\boldsymbol{L}}$ is the parameter related to the length of the tube.

The verification of the codes is essential to trust the results obtained from them. In many problems we try to consider cases with exact solutions and compare the solutions computed using the codes with the exact solutions of the problems. In our case, we do not know the exact solution, but we know the solution found and computed by Hammond in [9]. So, we compare all our results with the Hammond's one.

In the subsection 4.2, we check the numerical results and statements that we use in the subsection 4.1, related to the accuracy of the schemes, considering the linear case $\boldsymbol{H_t} = -\frac{\mathbf{1}}{\mathbf{3}}\boldsymbol{H_{zzzz}}$. This equation with the initial condition $\boldsymbol{H(z, 0)} = \mathbf{1} + \boldsymbol{\beta}\,\mathbf{cos}(\boldsymbol{z})$, has an exact solution expressed by $\boldsymbol{H(z, t)} = \mathbf{1} + \boldsymbol{\beta}\,\mathbf{cos}(\boldsymbol{z})\boldsymbol{e}^{-\frac{\mathbf{1}}{\mathbf{3}}\boldsymbol{t}}$.

4.1 Numerical experiments

In this section, we present the numerical experiments made using codes for the different numerical schemes previously proposed. It is known that the "FD schemes are somewhat inferior in accuracy compared to spectral schemes" [19], where FD stands for Finite Differences. This is clear from the fact that the pseudospectral methods have exponencial convergence, which makes them by far superior to the FD methods which expose algebraic convergence [10]. The error between a solution and its N–th order truncated Fourier series decays faster than algebraically in 1/N, when such solution is infinitely smooth and periodic with all its derivatives. This is known as the spectral accuracy, or infinite–order accuracy. In this case we say that the series has an infite–order convergence [3].

So first, we numerically solve the nonlinear equation (10) using all the numerical schemes considered in this work. We need to compute the relative errors in order to decide what method gives the best approximation to the exact solution; but we do not know the exact solution for this equation. However,

Hammond [9] solved it numerically; so, it would be natural to compare all the numerical solutions that we obtained, with the one already known and obtained by Hammond. In what follows, we present the comparisons.

4.1.1 Comparisons with Hammonds results In this subsection, we present all the numerical results obtained from the methods already explained in previous sections of this article, and we compare them with the numerical results obtained by Hammond. Thus, we solve (10) and (11) for times $\boldsymbol{T = 6, 18, 30, 60}$ and length $\boldsymbol{L = 6\pi}$ for the system, applying the pseudo–spectral methods, one with Euler's method and the other one with Runge–Kutta's method of fourth order. Also, we apply the finite difference methods, one explicit and the other one implicit.

We performed several runs using all the codes (EXPLI, IMPLI, SPEC–EU, and SPEC–RK) applied to Hammond's equation and compared them with the numerical solution obtained by Hammond [9].

In Figure 1, we present the graph corresponding to the modules of the differences between the numerical results obtained by using the implicit finite difference method and the Hammond's solution. We observe that the results are almost the same for all the times considered, except at the extremes where we can note that the differences increase as $\boldsymbol{T}$ increases. Thus, when $\boldsymbol{T = 60}$, the absolute error is **0.03131** and the relative error is by the order of **0.87%** which is good.

For the methods of pseudo–spectral with Euler and pseudo–spectral with Runge–Kutta of fourth order, we have found similar behaviors for the modules of the differences between the numerical results obtained from one of our methods and the Hammond's solution. We have found that the worse case happens for the explicit method when time increases.

In Table 1, we have the absolute and relative errors for the numerical results, obtained from all the methods we study in this article, comparing them with the Hammond's solution. The results are given for final time $\boldsymbol{T = 60}$, $\boldsymbol{N = 2^7}$, and $\boldsymbol{\Delta t = 10^{-4}}$. It can be observed that the pseudo–spectral methods (with Euler and Runge–Kutta of fourth order) produce solutions with relative errors by the order of **3.5%** (see rows **3** and **4**), while the implicit FD method produces a solution with relative error by the order of **0.87%** (see row **2**).

We can conclude that the implicit finite difference method gives the best approximation to the numerical solution obtained by Hammond. But this is a contradiction with the fact that the FD methods are inferior to the pseudospectral methods [19]. So, what is it happening? Can we trust our results? Let us analize the situation. Hammond used the method of lines to obtain the numerical solutions [9], but the method of lines is based on FD methods. Therefore, we can not trust the comparisons.

On the other hand, since the pseudo–spectral methods have infinite–order

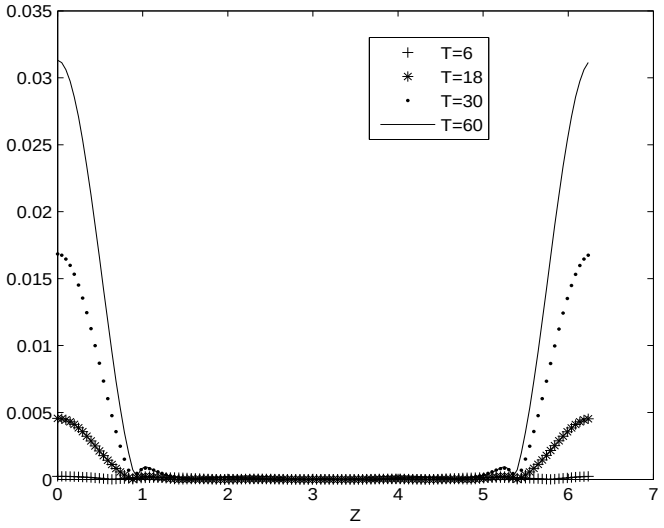

Figure 1: Profiles of the modules of the differences between the numerical results obtained by using the implicit finite difference method and the Hammond's solution.

convergence [3], see section 4.1 for comments, we decide to choose one of the pseudospectral methods considered in this article as the most accurate solution to the problem. It is known that the method of Runge–Kutta of fourth order is more accurate than the method of Euler, which is second order. So, from now on, we take the solution obtained from pseudo–spectral with Runge–Kutta's method of fourth order as the most accurate solution for the initial value problem (10) and (11) in this article, and do the comparisons.

4.1.2 Comparisons with results from pseudo–spectral with Runge–Kutta of fourth order In this subsection, we compare the numerical solutions obtained from our numerical methods, with the solution computed using the pseudo–spectral method with Runge–Kutta of fourth order; for an explanation, see subsection 4.1.1 and introduction to section 4.1.

In Figure 2 we present the profiles of the interface evolution obtained solving (10) and (11) using the pseudo–spectral with Runge–Kutta's method of fourth order. The profiles correspond to times $\boldsymbol{T = 6, 18, 30, 60}$, and $\boldsymbol{L = 6\pi}$. Here, the horizontal axis represents the tube wall. As we can observe in Figure 2, as time increases, the interface perturbation becomes higher and higher. Thus, the perturbed interface may eventually touch the tube wall; in this sense the

Table 1: Comparisons of the numerical solutions obtained applying the methods: explicit and implicit finite differences, pseudo–spectral with Euler and pseudo–spectral with Runge–Kutta of fourth order, with the Hammond's solution [9] for $\boldsymbol{N = 2^7}$, final time $\boldsymbol{T = 60}$ and $\boldsymbol{\Delta t = 10^{-4}}$.

Row	Code	Absolute error	Relative error
1	EXPLI	$\mathbf{1.019\ x10^{-1}}$	$\mathbf{9.132\ x10^{-1}}$
2	IMPLI	$\mathbf{3.131\ x10^{-2}}$	$\mathbf{8.744\ x10^{-3}}$
3	SPEC-EU	$\mathbf{8.554\ x10^{-2}}$	$\mathbf{3.531\ x10^{-2}}$
4	SPEC-RK	$\mathbf{8.482\ x10^{-2}}$	$\mathbf{3.535\ x10^{-2}}$

system becomes more unstable. So, from the profile for $\boldsymbol{T = 60}$, we may think about the possibility, for some time $\boldsymbol{T}$ in the future, of a contact of the interface with the tube wall. For this case, we could need to do another research and, of course, consider other numerical schemes to be able to capture the rupture of the interface.

In Figure 3, we present the graph corresponding to the modules of the differences between the numerical results obtained by using the pseudo–spectral methods studied in this article. We observe that the results are almost the same for all the times considered, except when $\boldsymbol{T = 60}$. In such a case, near the extremes the differences are by the order of $\mathbf{10^{-4}}$, which it is still acceptable. In Table 2, Row 3, we can see the precise values for the errors.

In the literature the implicit methods, in general, have been proved to be more effective than the explicit ones [16] in the sense that convergence happens with bigger steps than the ones required for the explicit methods. Thus, we compare the results obtained from the implicit finite difference method with those obtained by the pseudo–spectral with Runge–Kutta's method of fourth order. Therefore, we present in Figure 4, the graph corresponding to the modules of the differences between the results from the implicit finite difference method and those from the pseudo–spectral with Runge–Kutta's method of fourth order. In this graph we also can observe that bigger differences occur at the extremes, but now by the order of $\mathbf{10^{-2}}$. Also see Row 2 of Table 2 for details on the errors calculated for $\boldsymbol{Time = 60}$.

In Figure 5, we plot the modules of the differences between the results from the method of lines and those from the pseudo–spectral with Runge–Kutta's method of fourth order. Looking at this graph we can observe that it is very similar to that in Figure 4, bigger differences occur at the extremes, and by the order of $\mathbf{10^{-2}}$ too. Check Row 4 of Table 2 to see the values of the errors.

In Figure 6, we present the relative error of the numerical solution obtained from the pseudo–spectral with Euler's method, considering the solution from the pseudo–spectral with Runge Kutta's method of fourth order as the most accurate numerical solution of the problem, as was discussed in Section 4.1.1.

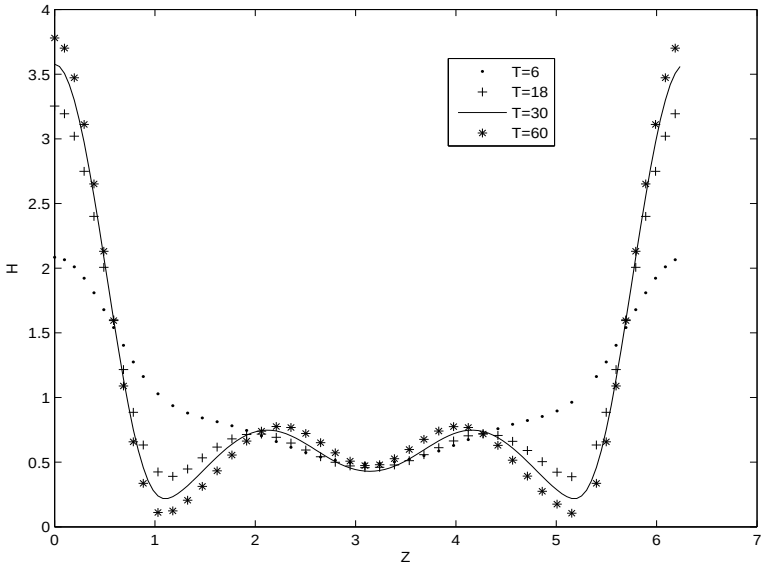

Figure 2: Profiles of the evolution of the interface using the pseudo–spectral with Runge Kutta's method of fourth order.

It can be easily observed that the relative error is by the order of $\mathbf{10^{-4}}$ which is excellent. See Row 3 in Table 2. This tells us that the pseudo–spectral with Euler's method produces a very good numerical solution.

On the other hand, in Figure 7, we plot the relative error of the numerical solution produced by the method of lines, considering, by the same reasons, that the solution from the pseudo–spectral with Runge Kutta's method of fourth order is the most accurate solution. It can be noted that the relative error is by the order of $\mathbf{10^{-2}}$. Also, in Table 2, we can observe that the method of lines (Row 4) and the implicit FD method (Row 2) produce very similar relative errors. The errors are by the order of $\mathbf{10^{-2}}$ which, even though it is also good, it tells us that the pseudo–spectral with Euler's method gives a better solution, with errors by the order of $\mathbf{10^{-4}}$, see Row 3.

All the results observed in Figures 3, 4, 5, 6, and 7, say that the numerical solution produced using the pseudo–spectral with Euler's method approximates the best the solution of the pseudo–spectral with Runge Kutta's method of fourth order. In what follows, we want to check the methods used in this article with some case in which we can have its exact solution. In order to do so, we consider the linear case of the Hammond's equation (10) which involves the higher order derivative of $\boldsymbol{H}$; then we calculate the exact solution to this linear equation. In the next step, we compute the numerical solutions using

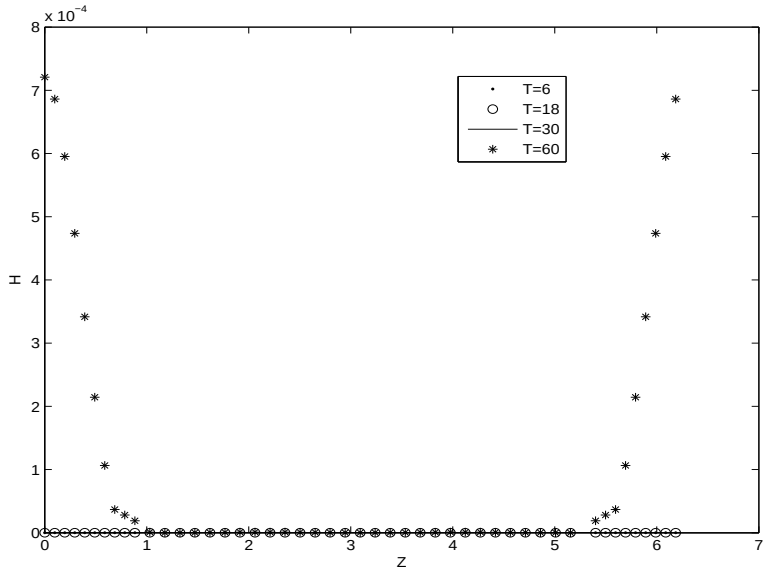

Figure 3: Module of the differences between the solutions from the pseudo–spectral with Euler's method and pseudo–spectral with Runge Kutta's method of fourth order.

all the methods proposed in this article that can be applied to this case, and determine which one of them is the best approximation to the exact solution. We also compare the numerical results with the one obtained by the method of lines.

4.2 Linear case

The linear form of (10) is given by

$$\boldsymbol{H_t = -\frac{1}{3} H_{zzzz}.} \tag{33}$$

We apply the pseudo–spectral with Euler's method (SPEC–EU) and the pseudo–spectral with Runge–Kutta's method of fourth order (SPEC–RK) to (33). From the finite difference methods, we use only the explicit method (EXPLI). The implicit scheme can not be applied to this equation because it does not have any nonlinear part, so the application of (22) and (23) is not possible.

The linear partial differential equation (33) is numerically solved for values of $\boldsymbol{z}$ in the interval $\boldsymbol{[0, 2\pi]}$ and $\boldsymbol{t}$ in the interval $\boldsymbol{[0, T]}$ under the initial condition

$$\boldsymbol{H(z, 0) = 1 + \beta \cos(z).} \tag{34}$$

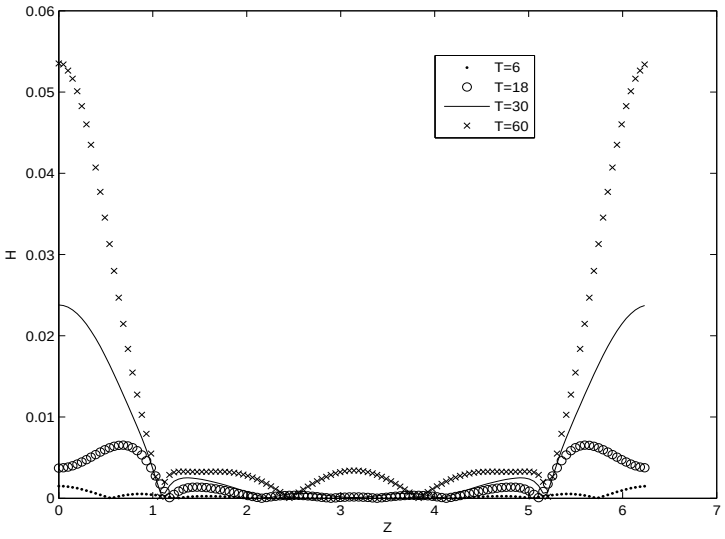

Figure 4: Module of the differences between the solutions from the implicit finite difference method and the pseudo–spectral with Runge Kutta's method of fourth order.

Also, we have verified each one of the codes for each corresponding method, applying them to the linear case. The codes were executed using several data sets and the numerical results obtained were compared with the exact solution of the initial value problem (33) and (34), which was determined using the method of separation of variables. The exact solution is expressed as follows:

$$\boldsymbol{H(z,t) = 1 + \beta \cos(z) e^{-\frac{1}{3}t}.} \tag{35}$$

With the purpose of comparing the numerical solutions with the exact one, we compute the absolute and relative errors. In order to calculate the absolute error, we use the norm $\| \cdot \|_\infty$ of the difference between the exact solution and the numerical solution calculated at each node. We compute the relative errors dividing the absolute errors by the exact solution. We present in Table 3 several results from where it can be observed what method gives the best approximation to the exact solution. This can be seen looking at the columns for the $\| \cdot \|_\infty$ error and the relative error.

From several runs performed in this section, we chose only sixteen of them, which are tabulated in Table 3. Here, we do not present comparative graphs since the differences between the exact solution (35) and the numerical solutions obtained from the pseudo–spectral methods, are undistinguishables. So, we

Table 2: Comparisons of the numerical solutions obtained applying the methods: explicit and implicit finite differences, pseudo–spectral with Euler and the method of lines, with the numerical solution from the method of pseudo–spectral with Runge–Kutta of fourth order for $\boldsymbol{N = 2^7}$, $\boldsymbol{\Delta t = 10^{-4}}$, and final time $\boldsymbol{T = 60}$.

Row	Code	Absolute error	Relative error
1	EXPLI	$\mathbf{1.835\ x10^{-1}}$	$\mathbf{9.335\ x10^{-1}}$
2	IMPLI	$\mathbf{5.351\ x10^{-2}}$	$\mathbf{3.632\ x10^{-2}}$
3	EXPEC-EU	$\mathbf{7.207\ x10^{-4}}$	$\mathbf{1.906\ x10^{-4}}$
4	LINE	$\mathbf{8.482\ x10^{-2}}$	$\mathbf{3.414\ x10^{-2}}$

limit the presentation of the results for this case to comparisons shown in Table 3.

Observing the Table 3, we can note that for the first four rows, which correspond to results for final time $\boldsymbol{T = 6}$, we have the relative errors: $\mathbf{9.919x10^{-3}}$ for the explicit FD method, $\mathbf{7.360x10^{-4}}$ for the method of lines, $\mathbf{4.838x10^{-6}}$ for the pseudo–spectral method with Euler, and $\mathbf{2.419x10^{-6}}$ for the pseudo–spectral method with Runge–Kutta of fourth order. For the next four rows, 5, 6, 7, and 8, which correspond to results for $\boldsymbol{T = 18}$, we can observe, once more, that the smallest relative error is obtained from the results given by the pseudo–spectral method with Runge–Kutta of fourth order. For time $\boldsymbol{T = 30}$, it is observed that the relative error using the method of lines is $\mathbf{7.416x10^{-6}}$, for the pseudospectral method with Euler, is $\mathbf{4.540x10^{-9}}$, and for the pseudospectral method with Runge–Kutta of fourth order, is $\mathbf{7.577x10^{-10}}$, which is the smallest relative error for this time too. When we run the codes for all the methods, at final time $\boldsymbol{T = 60}$, we obtain $\mathbf{1.544x10^{-3}}$, $\mathbf{2.268x10^{-7}}$, $\mathbf{3.440x10^{-12}}$, and $\mathbf{0.000x10^{-15}}$, for the explicit FD method, the method of lines, the pseudospectral method with Euler, and the pseudospectral method with Runge–Kutta of fourth order, respectively. For this time we can observe the spectral accuracy of the pseudospectral method with Runge–Kutta of fourth order.

On the other hand, for $\boldsymbol{N = 2^5}$, $\boldsymbol{\Delta t = 10^{-3}}$, and $\boldsymbol{T = 60}$, the execution times for the codes EXPLI, SPEC–EU, and SPEC–RK are 1.062, 3.04, and 25.89, respectively. This put the explicit and pseudo–spectral with Euler methods in advantage with respect to the pseudo–spetral method with Runge–Kutta of fourth order. When $\boldsymbol{N = 2^6}$, $\boldsymbol{\Delta t = 10^{-4}}$, and $\boldsymbol{T = 60}$, it is observed that EXPLI continue having the smallest execution time, then SPEC–EU follows with a bigger execution time, and finally SPEC–RK has the biggest one.

Thus, from our results we have checked that the pseudo–spectral with Runge–Kutta's method of fourth order produces the most accurate numerical solution, even though there is a computational cost to pay; it is followed, in accuracy,

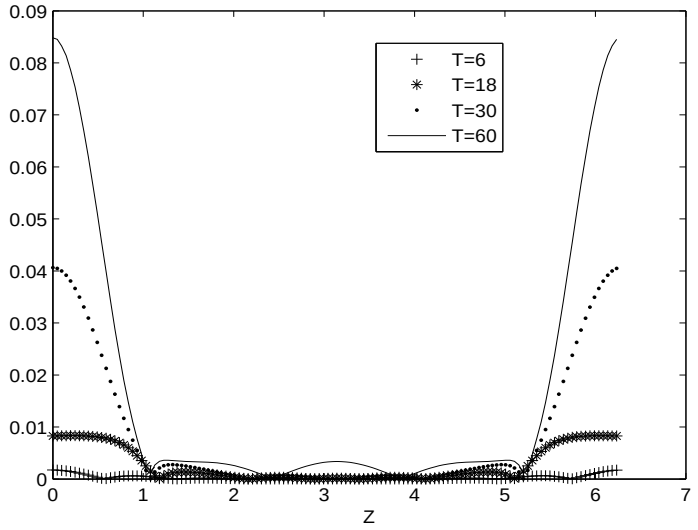

Figure 5: Module of the differences between the solutions from the method of lines and the pseudo–spectral with Runge Kutta's method of fourth order.

by the pseudo–spectral with Euler's method. This is in accordance with the fact that the pseudospectral methods have exponencial convergence [3], which makes them by far more accurate than the FD methods [10], [19], and with the known fact that the method of Runge–Kutta of fourth order produces more accurate solutions than the method of Euler. So, we have checked that there is no problem to consider, in this article, the solution from the pseudo–spectral method with Runge–Kutta of fourth order as the most accurate solution for the problem (10) and (11).

5 Conclusions

Since the pseudo–spectral methods have infinite–order convergence [3], see Section 4.1 for comments, and the method of Runge–Kutta of fourth order is more accurate than the method of Euler, we decided to choose the pseudo–spectral with Runge–Kutta's method of fourth order as the most accurate solution for the initial value problem (10) and (11), in this article.

The horizontal axis represents the tube wall. As we can observe in Figure 2, as time increases, the interface perturbation becomes higher and higher. Thus, the perturbed interface may eventually touch the tube wall; in this sense the

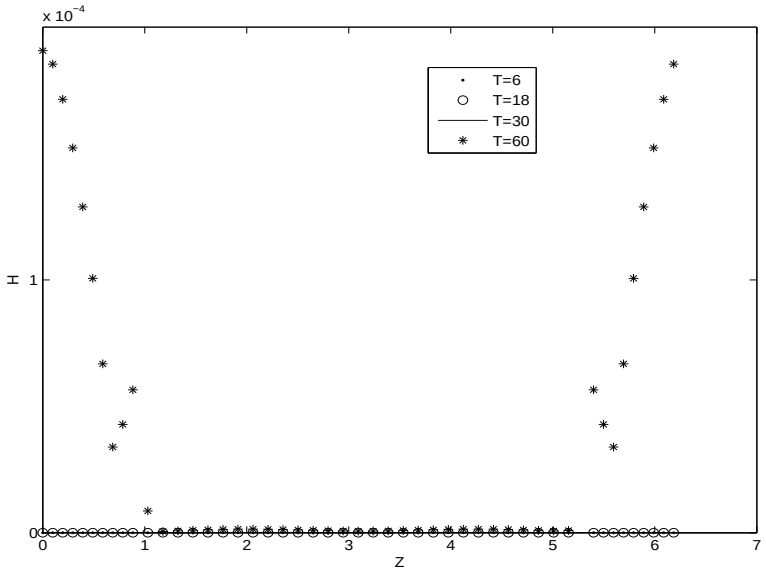

Figure 6: Relative error of the solution obtained by the pseudo–spectral with Euler's method.

system becomes more unstable. Therefore, from the profile for T = 60, we may think about the possibility, for some time T in the future, of a contact of the interface with the tube wall. For this case, we could need to do another research and, of course, consider other numerical schemes to be able to capture the rupture of the interface.

We observe, see Figure 3, that the numerical results obtained by using the two pseudo–spectral methods, used in this article, are almost the same for all the times considered, except when T = 60. In such a case, near the extremes the differences are by the order of $\mathbf{10^{-4}}$, which it is very good.

In the literature the implicit methods, in general, have been proved to be more effective than the explicit ones [16] in the sense that convergence happens with bigger steps than the ones required for the explicit methods. Thus, we compare the results obtained from the implicit finite difference method with those obtained by the pseudo–spectral with Runge–Kutta's method of fourth order. Therefore, in Figure 4, we can observe that bigger differences occur at the extremes, by the order of $\mathbf{10^{-2}}$.

The differences between the results from the method of lines and those from the pseudo–spectral with Runge–Kutta's method of fourth order, see Figure 5, are noted at the extremes, and by the order of $\mathbf{10^{-2}}$ too.

In Figure 6, we present the relative error of the numerical solution obtained

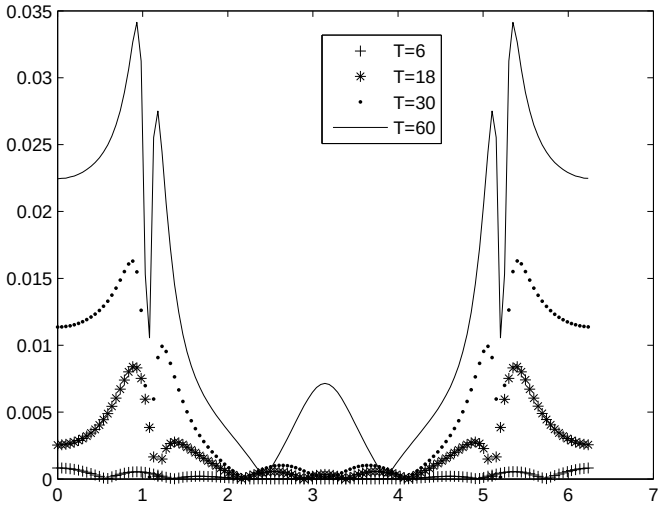

Figure 7: Relative error of the solution obtained by the method of lines.

from the pseudo–spectral with Euler's method, considering the solution from the pseudo–spectral with RungeKutta's method of fourth order as the most accurate numerical solution of the problem. It can be easily observed that the relative error is by the order of $\mathbf{10^{-4}}$ which is excellent. Thus, the pseudo–spectral with Euler's method produces a very good numerical solution.

On the other hand, the relative error of the numerical solution produced by the method of lines is by the order of $\mathbf{10^{-2}}$, considering, by the same reasons, that the solution from the pseudo–spectral with RungeKutta's method of fourth order is the most accurate solution.

Considering the linear form of (10), we apply the pseudo–spectral with Euler's method (SPEC–EU) and the pseudo–spectral with Runge–Kutta's method of fourth order (SPEC–RK) to (33). From the finite difference methods, we use only the explicit method (EXPLI). The implicit finite difference scheme cannot be applied to this equation because it does not have any nonlinear part, so the application of our implicit scheme (22) and (23) is not possible here. We have verified each one of the codes for each corresponding method, applying them to the linear case. The codes were executed using several data sets and the numerical results obtained were compared with the exact solution of the initial value problem (33) and (34), which was determined using the method of separation of variables. With the purpose of comparing the numerical solutions with the exact one, we compute the absolute and relative errors.

Table 3: Comparisons of the exact solution (35) with the numerical solutions obtained applying the following methods: explicit finite differences, lines, pseudo–spectral with Euler and pseudo–spectral with Runge–Kutta of fourth order for $\boldsymbol{N = 2^5}$, $\boldsymbol{\Delta t = 10^{-4}}$ and different final times, $\boldsymbol{T}$.

Row	T	Code	Absolute error	Relative error
1	6	EXPLI	$\mathbf{1.059\ x10^{-2}}$	$\mathbf{9,919\ x10^{-3}}$
2	6	LINE	$\mathbf{6,863\ x10^{-4}}$	$\mathbf{7,360\ x10^{-4}}$
3	6	ESPEC–EU	$\mathbf{4,511\ x10^{-6}}$	$\mathbf{4,838\ x10^{-6}}$
4	6	ESPEC–RK	$\mathbf{2,255\ x10^{-6}}$	$\mathbf{2,419\ x10^{-6}}$
5	18	EXPLI	$\mathbf{2,002\ x10^{-3}}$	$\mathbf{1,999\ x10^{-3}}$
6	18	LINE	$\mathbf{9,692\ x10^{-6}}$	$\mathbf{9,680\ x10^{-6}}$
7	18	ESPEC–EU	$\mathbf{1,652\ x10^{-7}}$	$\mathbf{1,654\ x10^{-7}}$
8	18	EXPEC–RK	$\mathbf{4,131\ x10^{-8}}$	$\mathbf{4,136\ x10^{-8}}$
9	30	EXPLI	$\mathbf{1,556\ x10^{-3}}$	$\mathbf{1,557\ x10^{-3}}$
10	30	LINE	$\mathbf{7,414\ x10^{-6}}$	$\mathbf{7,416\ x10^{-6}}$
11	30	EXPEC–EU	$\mathbf{4,539\ x10^{-9}}$	$\mathbf{4,540\ x10^{-9}}$
12	30	EXPEC–RK	$\mathbf{7,566\ x10^{-10}}$	$\mathbf{7,577\ x10^{-10}}$
13	60	EXPLI	$\mathbf{1,544\ x10^{-3}}$	$\mathbf{1,544\ x10^{-3}}$
14	60	LINE	$\mathbf{2,268\ x10^{-7}}$	$\mathbf{2,268\ x10^{-7}}$
15	60	EXPEC–EU	$\mathbf{3,440\ x10^{-12}}$	$\mathbf{3,440\ x10^{-12}}$
16	60	EXPEC–RK	$\mathbf{0,000\ x10^{-15}}$	$\mathbf{0,000\ x10^{-15}}$

From the results obtained using all the methods considered in this article, at final time T = 60, we can observe the spectral accuracy of the pseudo–spectral method with Runge–Kutta of fourth order with an error of order $\mathbf{10^{-15}}$. Thus, from our results, we have checked that the pseudo–spectral with Runge–Kutta's method of fourth order produces the most accurate numerical solution, even though there is a computational cost to pay; it is followed, in accuracy, by the pseudo–spectral with Euler's method. This is in accordance with the fact that the pseudo–spectral methods have exponencial convergence [3], which makes them by far more accurate than the finite difference methods [10], [19], and with the known fact that the method of Runge–Kutta of fourth order produces more accurate solutions than the method of Euler.

Therefore, considering that the numerical solution obtained from the pseudo–spectral with Runge Kutta's method of fourth order is the most accurate numerical solution of the problem, we took it as the reference solution for the nonlinear problem, and conclude that the pseudo–spectral with Euler's method produces the best numerical solution to the problem (10) and (11) for times $\boldsymbol{T = 6, 18, 30, 60}$ and length $\boldsymbol{L = 6\pi}$.

Acknowledgments

RG thanks the Consejo de Desarrollo Científico y Tecnológico (CDCHT) of the Universidad de Los Andes for financing this work through the project I 10440705b. SK thanks the Consejo de Investigación of the Universidad de Oriente for financing the project CI–2–010301–1277/06.

References

[1] R. L. BURDEN AND J. D. FAIRES, (1997), *Numerical Analysis, Sixth edition*, Brooks/Cole Publishing Company.

[2] C. CANUTO, M. Y. HUSSAINI, A. QUARTERONI AND T. A. ZANG, (1988), *Spectral Methods in Fluid Dynamics*, Springer Series in Computational Physics, Springer–Verlag, USA.

[3] C. CANUTO, M. Y. HUSSAINI, A. QUARTERONI AND T. A. ZANG, (2006), *Spectral Methods. Fundamentals in Single Domains*, Scientific Computation, Springer, USA.

[4] K. CHEN, R. BAI AND D. D. JOSEPH, *Lubricated pipelining. Part 3. Stability of core–anular flow,* Journal of Fluid Mechanics, 214, (1990), pp. 251–286.

[5] T. J. CHUNG, (2002), *Computational Fluid Dynamics*, Cambridge University Press.

[6] P. A. GAUGLITZ AND C. J. RADKE, *An extended evolution equation for liquid film breakup in cylindrical capillaries,* Chemical Engineering Science, 43, (1988), pp. 1457–1465.

[7] S. L. GOREN, *The instability of anular thread of fluid*, Journal of Fluid Mechanics, 12, (1962), pp. 309–319.

[8] D. GOTTLIEB AND S. A. ORSZAG, (1993), *Numerical Analysis of Spectral Methods: Theory ans Applications, Sixth printing*, SIAM, Capital City Press.

[9] P. S. HAMMOND, *Nonlinear adjustament of a thin annular film of viscous fluid surrounding a thread of another within a circular cylindrical pipe*, J. Fluid Mech. (1983), 137, pp. 363–384.

[10] H. HOLMÅS, D. CLAMOND AND H. P. LANGTANGEN, *A pseudospectral Fourier method for a 1D incompressible two–fluid model*, International Journal for Numerical Methods in Fluids (2008), 58, pp. 639–658.

[11] H. P. HSU, *Análisis de Fourier* , Addison Wesley Longman.

[12] S. A. KAS–DANOUCHE, (2002), *Nonlinear interfacial stability of core–annular film flows in the presence of surfactans,* Ph.D. Dissertation, New Jersey Institute of Technology and Rutgers, The State University of New Jersey – Netwark.

[13] S. A. KAS–DANOUCHE, D. T. PAPAGEORGIOU AND M. SIEGEL, *A mathematical model for core–annular flows with surfactants,* Divulgaciones Matemáticas, Vol 12, N 2, (2004), pp. 117–138.

[14] S. A. KAS–DANOUCHE, *A mathematical model for core–annular fluids with surfactants,* Boletín de la Asociación Matemática Venezolana, Vol XIV, N 1 y 2, (2007), pp. 27–39.

[15] S. A. KAS–DANOUCHE, D. T. PAPAGEORGIOU AND M. SIEGEL, *Nonlinear dynamics of core–annular film flows in the presence of surfactant,* Journal of Fluid Mechanics, 626, (2009), pp. 415–448.

[16] D. KINCAID AND W. CHENEY, (1996), *Numerical Analysis*, second edition, Brooks/Cole Publishing Company.

[17] C. KOURIS AND J. TSAMOPOULOS, *Dynamics of axisymmetric core–annular flow in a strtaight tube. I. The more viscous fluid in the core, bamboo waves*, Physics of Fluids, 13 (2002), pp. 1011–1029.

[18] K. W. MORTON AND D. F. MAYERS, (1994), *Numerical Solutions of Partial Differential Equations*, Cambridge University Press.

[19] V. NAULIN AND A. NIELSEN, *Accuracy of spectral and finite difference schemes in 2D advection problems,* SIAM Journal Sci. Comput., Vol 25, N 1, (2003), pp. 104–126.

[20] W. H. PRESS, S. A. TEUKOLSKY, W. T. VETERLING, AND B. P. FLANNERY, (1992), *Numerical Recipes In Fortran 77: The art of Scienctific Computing* (Vol 1 of Fortran Numerical Recipes), Cambridge University Press, New York.

[21] Y. Y. RENARDY, *Snakes and corkscrews in core–annulardown–flow of two fluids*, Journal of Fluid Mechanics, 340, (1997), pp. 297–317.

[22] A. RUTHERFORD, (1962), *Vectors, Tensors, and the Basics Equations of Fluid Mechanics*, Dover Publications, Inc, New York.

[23] J. C. STRIKWERDA, (1989), *Finite Difference Schemes and Partial Differential Equations*, Chapman and Hall.

[24] THOMAS AND FINNEY, (1996), *Calculus*, Addison Wesley.

[25] G. L. TAYLOR, Journal of Fluid Mechanics, 10, (1961), p. 161.

[26] S. TOMOTIKA *On the instability of a cylindrical thread of a viscous liquid surrounded by another viscous liquid,* Proc. R. Soc. Lond. A, 150 (1935), pp. 322–337.

Rodolfo Gallo
Departamento de Cálculo, Escuela Básica,
Facultad de Ingeniería,
Universidad de Los Andes, Mérida, Venezuela.

Said Kas–Danouche
Laboratorio de Alto Cómputo,
Departamento de Matemáticas, Escuela de Ciencias,
Núcleo de Sucre, Universidad de Oriente, Cumaná, Venezuela.

e-mail: rodolfog@ula.ve, sak0525@gmail.com